Europace (2005) **7**, S166–S177

ELSEVIER

EUROPEAN SOCIETY OF CARDIOLOGY®

Computer simulations of successful defibrillation in decoupled and non-uniform cardiac tissue

N.H.L. Kuijpers [a,*], R.H. Keldermann [b], T. Arts [a,c], P.A.J. Hilbers [a]

[a] *Department of Biomedical Engineering, Technische Universiteit Eindhoven, P.O. Box 513, 5600 MB Eindhoven, The Netherlands*
[b] *Department of Theoretical Biology, Universiteit Utrecht, Padualaan 8, 3584 CH Utrecht, The Netherlands*
[c] *Department of Biophysics, Universiteit Maastricht, P.O. Box 616, 6200 MD Maastricht, The Netherlands*

Submitted 15 January 2004, and accepted after revision 3 May 2005

Downloaded from by guest on July 25, 2016

KEYWORDS
bidomain model;
field stimulation;
defibrillation;
spiral wave;
virtual electrode polarization

Abstract **Aim** The aim of the present study is to investigate the origin and effect of virtual electrode polarization in uniform, decoupled and non-uniform cardiac tissue during field stimulation.
Methods A discrete bidomain model with active membrane behaviour was used to simulate normal cardiac tissue as well as cardiac tissue that is decoupled due to fibrosis and gap junction remodelling. Various uniform and non-uniform electric fields were applied to the external domain of uniform, decoupled and non-uniform resting cardiac tissue as well as cardiac tissue in which spiral waves were induced.
Results Field stimulation applied on non-uniform tissue results in more virtual electrodes compared with uniform tissue. The spiral waves were terminated in decoupled tissue, but not in uniform, homogeneous tissue. By gradually increasing local differences in intracellular conductivities, the amount and spread of virtual electrodes increased and the spiral waves were terminated.
Conclusion Fast depolarization of the tissue after field stimulation may be explained by intracellular decoupling and spatial heterogeneity present in normal and pathological cardiac tissue. We demonstrated that termination of spiral waves by means of field stimulation can be achieved when the tissue is modelled as a non-uniform, anisotropic bidomain with active membrane behaviour.
© 2005 The European Society of Cardiology. Published by Elsevier Ltd. All rights reserved.

* Corresponding author. Tel.: +31 40 247 4448; fax: +31 40 247 2740.
E-mail address: n.h.l.kuijpers@tue.nl (N.H.L. Kuijpers).

1099-5129/$30 © 2005 The European Society of Cardiology. Published by Elsevier Ltd. All rights reserved.
doi:10.1016/j.eupc.2005.03.021

Introduction

Defibrillation is a common clinical procedure to terminate atrial and ventricular fibrillation. An externally applied electric field leads to the development of so-called virtual electrode polarization, or VEP [1]. The VEP can affect the transmembrane potential: new action potentials can arise or existing action potentials can be prolonged or shortened [2]. When defibrillation is successful, the entire tissue depolarizes within a short time and after recovery sinus rhythm is restored [3]. In this study we investigate the origin of the VEP in uniform, decoupled and non-uniform cardiac tissue by means of computer simulations. Furthermore, we investigate the role of the VEP in relation to the termination of a spiral wave in normal as well as pathological tissue.

Computer simulations of defibrillation require a model that distinguishes between the intracellular and extracellular domains. If the rates of anisotropy for the intracellular and extracellular domains are modelled differently, virtual electrodes appear in the vicinity of both the cathode and the anode [4]. These observations have been verified experimentally [5]. However, in computer simulations using a continuous bidomain model, virtual electrodes do not appear in the bulk of the tissue and cannot explain depolarization of the entire tissue within a short time.

Several groups have used discontinuous bidomain models to investigate the effect of structural non-uniformities in cardiac tissue when external electric fields are applied [6]. In some of these models the effects of the gap junctions are incorporated by modelling periodic changes in the internal conductivities [7,8]. In simulations using these models, so-called ''sawtooth'' patterns appear in spatial mappings of the transmembrane potential [9]. Although they have been searched for, these ''sawtooth'' patterns have not been observed experimentally [10]. Also in cultured layers of myocytes, no virtual electrodes were observed at the cell borders [11]. Later bidomain models focus on modelling fibre curvature both in 2D and 3D [12]. Using these models, virtual electrodes appeared further away from the physical electrodes and spiral waves have been terminated [13].

In a study by Fast et al. using directed cell growth in cell cultures with intercellular clefts, large changes in the transmembrane potential have been observed at the boundaries of cell strands and at the intercellular clefts [14]. Secondary sources of stimulation, i.e., depolarization of tissue not directly caused by the stimulating electrodes, have also been found near surgical incisions in dog hearts [15]. A bidomain model describing the laminar organization of myocytes has been used to investigate the effect of an external electric field applied to the ventricular wall of a rat [16]. In these simulations, the bulk of the tissue was depolarized in regions located near the interlaminar clefts [16].

In a simulation study by Fishler the effect of spatial heterogeneity during monophasic and biphasic shocks was investigated by varying the intracellular volume fraction randomly throughout the tissue [17,18]. In another study by Krassowska the effect of spatial heterogeneity was statistically investigated by varying cell length, cell diameter, thickness of the extracellular space and the junctional resistances in 10 different random fibres [19]. Both studies indicate a decrease in the field stimulation threshold as a consequence of spatial heterogeneity.

Keener and Cytrynbaum investigated defibrillation in a 1D ring and a 2D sheet using dynamical systems theory [20]. In their study spatial heterogeneity was modelled at different scales. They conclude that spatial inhomogeneity, especially at smaller scales, leads to an increase in the success rate of defibrillation [20]. Very recently, Plank et al. investigated the effect of spatial heterogeneity and the level of organization of fibrillating tissue in relation to the defibrillation shock strength [21]. They concluded that the required shock strength for successful defibrillation increases with disorganization of the fibrillatory state [21]. Similar observations were also made by Hillebrenner et al. [22].

The aim of the present study is to obtain more insight in the role of decoupling and non-uniform conductivities in the clinical success of defibrillation. To simulate virtual electrode polarization as a consequence of field stimulation, we use a discrete bidomain model, which is aimed at irregular conductivity properties of cardiac tissue at the cellular level. To study the effects of decoupling and non-uniformity, conductivities between adjacent cells are randomly varied. In order to model the membrane behaviour of individual atrial myocytes, we apply the Human Atrial Action Potential Model as developed by Courtemanche et al. [23]. Electroporation is modelled as described by Aguel et al. [24]. Computer simulations of various rectangular sheets of atrial tissue have been performed to investigate the effect of non-uniformity and decoupling when an external electric field is applied. To investigate the success of

Downloaded from by guest on July 25, 2016

defibrillation, spiral waves were induced on a sheet of 8 cm × 3 cm cardiac tissue using an S1S2 protocol [13]. We hypothesize that fast depolarization of the entire tissue after field stimulation is related to the amount of decoupling and non-uniformity in the tissue.

Methods

Cellular Bidomain Model

The discrete bidomain model we use is called the Cellular Bidomain Model. Both the electrical behaviour of the cell membrane and the propagation of the depolarization wave are described by this model. The structure of the cardiac tissue is represented by a *graph* consisting of nodes and edges, where a *node* represents a group of cells and an *edge* the electrical connections between the cells. Such a graph is called a *simulation graph* and is denoted by $G(N,E)$, where N is the set of nodes and E the set of edges connecting the nodes.

Within a simulation graph, a number of different cell types can be distinguished, e.g., sino-atrial node cells and atrial myocytes, each having their own membrane behaviour. The state of each node $n \in N$ is defined by the *internal potential* V^n_{int}, the *external potential* V^n_{ext} and the state of the cell membrane. The membrane potential is defined as the difference between the internal and external potential, i.e., $V^n_{\text{mem}} = V^n_{\text{int}} - V^n_{\text{ext}}$. Edges define the conductivity properties for intracellular and extracellular currents between two adjacent nodes. We distinguish the *internal* and *external conductivity*, which are denoted by σ_{int} and σ_{ext}, respectively. We assume that the simulation graph is not directed and for edge $(n,m) \in E$ connecting nodes n and m it is assumed that $\sigma^{(n,m)}_{\text{int}} > 0$ and $\sigma^{(n,m)}_{\text{ext}} > 0$. The internal and external currents flowing from node n to node m are denoted by $I^{n\to m}_{\text{int}}$ and $I^{n\to m}_{\text{ext}}$, and are given by Ohm's law:

$$I^{n\to m}_{\text{int}} = \left(V^n_{\text{int}} - V^m_{\text{int}}\right)\sigma^{(n,m)}_{\text{int}}, \tag{1}$$

$$I^{n\to m}_{\text{ext}} = \left(V^n_{\text{ext}} - V^m_{\text{ext}}\right)\sigma^{(n,m)}_{\text{ext}}. \tag{2}$$

The intracellular current entering node n coming from all adjacent nodes a, $(n,a) \in E$, is denoted by I^n_{int}. The extracellular current entering node n is denoted by I^n_{ext}, i.e.,

$$I^n_{\text{int}} = \sum_{(n,a)\in E} I^{a\to n}_{\text{int}}, \tag{3}$$

$$I^n_{\text{ext}} = \sum_{(n,a)\in E} I^{a\to n}_{\text{ext}}. \tag{4}$$

According to Kirchhoff's law, current entering a node as intracellular current must leave as extracellular current, thus

$$I^n_{\text{int}} + I^n_{\text{ext}} = 0. \tag{5}$$

Furthermore, the transmembrane current for node n, denoted by I^n_{trans}, is the sum of capacitive and ionic currents, i.e.,

$$I^n_{\text{trans}} = C^n_{\text{mem}}\frac{\mathrm{d}V^n_{\text{mem}}}{\mathrm{d}t} + S^n_{\text{mem}} I_{\text{ion}}\left(V^n_{\text{mem}}, \mathbf{q}^n\right) = I^n_{\text{int}}, \tag{6}$$

where C^n_{mem} represents the membrane capacitance of node n in μF, and S^n_{mem} the membrane surface in cm^2. The ionic membrane current of node n is denoted by $I_{\text{ion}}\left(V^n_{\text{mem}}, \mathbf{q}^n\right)$ and is expressed in μA per cm^2 membrane surface. The ionic current depends on the membrane potential and the state of the membrane, which is usually described by a number of gating variables. The set of variables describing the membrane state is denoted by $\mathbf{q}^n$. The membrane state depends on the membrane potential:

$$\frac{\mathrm{d}\mathbf{q}^n}{\mathrm{d}t} = M_{\text{ion}}\left(V^n_{\text{mem}}, \mathbf{q}^n\right). \tag{7}$$

The ionic membrane current modelled by functions I_{ion} and M_{ion} can be implemented by any membrane model [23,25,26]. Different membrane models can be applied for different nodes to model heterogeneous cell membrane behaviour of the cardiac tissue.

In this study we use a brick wall structure to model the cardiac myocytes. Each node represents a rectangular piece of tissue of length 200 μm and width 80 μm lying in the direction of the fibres (see Fig. 1). Note that the bricks are not subdivided into smaller parts: the same state is assumed throughout the entire brick. In order to obtain conduction velocities within physiological range [27], we have rescaled the conductivity parameters as reported by Clerc [28] with a factor 0.6. The tissue parameters used in the present study are listed in Table 1. These parameters result in a conduction velocity of 0.41 m/s along the fibre direction and 0.13 m/s across the fibre direction.

The membrane behaviour for each node is simulated by the Human Atrial Action Potential Model as developed by Courtemanche et al. [23]. The equations of the Cellular Bidomain Model

Downloaded from by guest on July 25, 2016

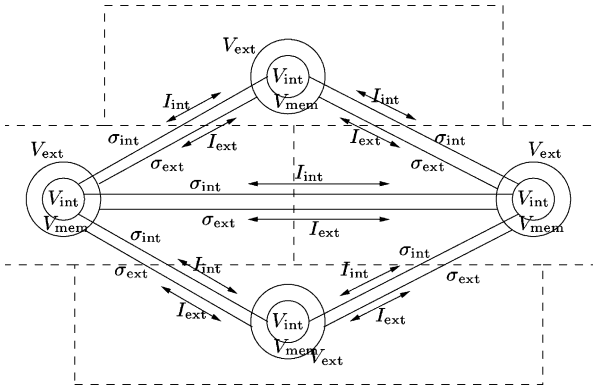

Figure 1 Graphical representation of a simulation graph. Each node represents a rectangular piece of cardiac tissue. The state of each node is represented by the internal potential V_{int}, the external potential V_{ext}, and the membrane potential V_{mem}. Electrical connections between the nodes are indicated by the intracellular and interstitial conductivities denoted by σ_{int} and σ_{ext}. The intracellular and interstitial current flowing between the nodes are represented by the arrows labeled I_{int} and I_{ext}.

are solved using a forward Euler scheme with a simulation time step of 0.010 ms. Below, we describe how electroporation, non-uniform conductivities and field stimulation are modelled.

Electroporation

When applying a large electric field on cardiac tissue, the membrane of cells near the electrodes start to electroporate [29], i.e., the membrane conductance is increased by the formation of aqueous pores [30]. Electroporation prevents membrane potentials from reaching extreme values [29].

We model electroporation as described by Aguel et al. [24]. The membrane behaviour of the Cellular Bidomain Model has been extended with an extra state variable G, denoting the pore generation in the membrane. Eq. (6) is adapted as follows [31]:

Table 1 Tissue parameters

Parameter	Value
Longitudinal internal conductivity, g^x_{int}	1.0440 mS/cm
Transverse internal conductivity, g^y_{int}	0.1158 mS/cm
Longitudinal external conductivity, g^x_{ext}	3.7500 mS/cm
Transverse external conductivity, g^y_{ext}	1.4160 mS/cm
Membrane capacitance, C_{mem}	1.0 μF/cm^2
Surface-to-volume ratio, χ	2000 cm^{-1}

$$I^n_{trans} = C^n_{mem}\frac{dV^n_{mem}}{dt} + S^n_{mem}\left(I_{ion}\left(V^n_{mem}, \mathbf{q}^n\right) + GV^n_{mem}\right) = I^n_{int}. \quad (8)$$

G is described by [31]:

$$\frac{dG}{dt} = \alpha e^{\beta\left(V^n_{mem}-V^n_{rest}\right)^2}\left(1 - e^{-\gamma\left(V^n_{mem}-V^n_{rest}\right)^2}\right), \quad (9)$$

where $\alpha = 2.5 \times 10^{-3}$ mS/cm^2 ms, $\beta = 2.5 \times 10^{-5}$ mV^{-2} and $\gamma = 1.0 \times 10^{-9}$ mV^{-2} [31]. V_{rest} represents the resting membrane potential, which is near -81 mV for the Human Atrial Action Potential Model [23]. Initially, G is set to 0 mS/cm^2.

Gap junctions

Gap junctions provide the pathways for intracellular current flow. The anisotropic conduction properties of the myocardium are dependent on the geometry of the intercalated disks and the number, size and location of the gap junctions in between them [32]. Changes in gap junction distribution are common in elderly people and are involved in the initiation and persistence of various cardiac arrhythmias [33].

In the Cellular Bidomain Model a distinction is made between *longitudinal* edges and *transverse* edges. The internal conductivities of the longitudinal edges represent the gap junctions between cells of the same fibre, whereas the internal conductivities of the transverse edges represent the gap junctions responsible for side-to-side coupling. The effects of gap junction remodelling are simulated by randomly changing the internal conductivities. A normal distribution (μ,σ) is applied to determine the factor by which the standard values for the internal conductivities are multiplied for each edge. In the sequel, the average and standard deviation of the gap junction remodelling factor in longitudinal direction are denoted by μ_L and σ_L, respectively, and the average and standard deviation in transverse direction by μ_T and σ_T, respectively.

Fibrosis

Fibrosis causes the loss of side-to-side cell coupling which may result in a disturbed wavefront propagation and can isolate groups of myocytes [34]. The development of fibrosis is associated with changes in the topology and number of gap junctions [27]. Since side-to-side coupling is affected, fibrosis leads to a reduction of the conduction velocity, mainly in transverse direction [27].

Downloaded from by guest on July 25, 2016

In the Cellular Bidomain Model, diffuse fibrosis [35] is simulated by removing the internal conductivities of some of the transverse edges. The so-called *fibrosis fraction* determines the number of affected transverse edges, but which transverse edges are affected is randomly determined. In the sequel, the fibrosis fraction is denoted by FF.

Simulation protocol

To investigate virtual electrode polarization on uniform, decoupled and non-uniform tissue, we modelled a 1 cm $\times$ 0.5 cm sheet of atrial tissue. A non-uniform electric field was established during 1 ms by placing the anode in the left upper quarter of the tissue and the cathode in the right lower quarter of the tissue. The strength of the electric field was varied using an anode voltage of $+1$, $+5$ and $+10$ V, respectively, and a cathode voltage of -1, -5 and -10 V, respectively. This protocol was applied to uniform, decoupled and non-uniform tissue. Decoupled tissue was modelled as uniform tissue in which artificial obstacles were placed. These obstacles were either non-conductive in the internal domain only, or they were non-conductive in both domains. Non-uniform tissue was modelled by multiplying the internal conductivities by a factor drawn from a normal distribution (μ,σ), with average $\mu = 1$ and standard deviation $\sigma = 0.5$, 1 and 1.5, respectively. These factors were bound with minimum 0.75, 0.5 and 0, respectively, and maximum 1.25, 1.5 and 2, respectively.

Two large-scale simulations of an 8 cm $\times$ 3 cm sheet of atrial tissue with and without fibrosis and gap junction remodelling were performed. In this case the cardiac tissue was divided into 150,000 bricks of size 200 μm $\times$ 80 μm. Pathological tissue was simulated with fibrosis fraction FF = 0.35 and average gap junction remodelling factor $\mu_L = \mu_T = 0.5$ and standard deviation $\sigma_L = \sigma_T = 1$. The conduction velocity in pathological tissue decreased from 0.41 to 0.19 m/s along the fibre direction and from 0.13 to 0.05 m/s across the fibre direction. To investigate the effect of non-uniform conductivity during defibrillation in normal tissue, the internal conductivities were changed before the electric field was applied. All internal conductivities were multiplied by a factor drawn from a normal distribution (μ,σ) with average $\mu = 1$ and standard deviation $\sigma = 0.5$ and 1, respectively. In both cases the factors were bound with minimum 0.75 and 0.5, respectively, and maximum 1.25 and 1.5, respectively.

An electric field was established during 10 ms by placing the anode at the top row of the tissue and the cathode at the bottom. The anode voltage was $+25$ V and the cathode voltage -25 V, generating a uniform electric field of 16.7 V/cm in the direction across the fibres. A similar protocol was used by Trayanova and Skouibine [13]. Field stimulation was applied on uniform and non-uniform normal tissue as well as pathological tissue in the resting state. For the final series of simulations, a spiral wave was induced in both normal and pathological tissue using an S1S2 stimulation protocol as described by Trayanova and Skouibine [13]. Each simulation lasted several seconds to let a spiral wave develop before field stimulation was applied.

Results

Anodal and cathodal point stimulation in uniform tissue results in the characteristic dog bones near the physical electrodes. For all three different strengths of the electric field, depolarization occurred near the cathode. Only in case of the two stronger electric fields, virtual electrodes near the anode lead to depolarization. No secondary sources were observed on larger distances from the physical electrodes. In Fig. 2 the results are shown for anode voltage $+10$ V and cathode voltage -10 V in uniform and decoupled tissue. The dog bone is clearly visible in the left column (uniform tissue). Secondary sources appear near the artificial obstacles (centre and right column). Note that the location of the secondary sources is different for internally uncoupled tissue (centre column) and fully uncoupled tissue (right column).

In Fig. 3 the results are shown for anodal and cathodal point stimulation in non-uniform tissue. The results are shown for the simulation runs with anode voltage $+10$ V and cathode voltage -10 V. The dog bone is clearly visible in the left column, but less apparent in the centre and right column. Furthermore, a larger number of virtual electrodes is present in the bulk of the tissue in the centre and right column. Virtual electrode polarization facilitates faster depolarization of the entire tissue. This can be clearly observed in the centre column of Fig. 2 and in the centre and right column of Fig. 3.

In Fig. 4 the results are shown when a uniform electric field is applied during 10 ms on normal, resting cardiac tissue. In uniform normal tissue (left column) cells depolarize in the vicinity of the two electrodes, but not in the bulk of the tissue. In non-uniform normal tissue (centre column) more virtual electrodes are present in the bulk of the tissue. The virtual electrodes either depolarize or hyperpolarize cells in their vicinity. In the right column, more virtual electrodes originate that are better spread over the tissue. The result is that the

Downloaded from by guest on July 25, 2016

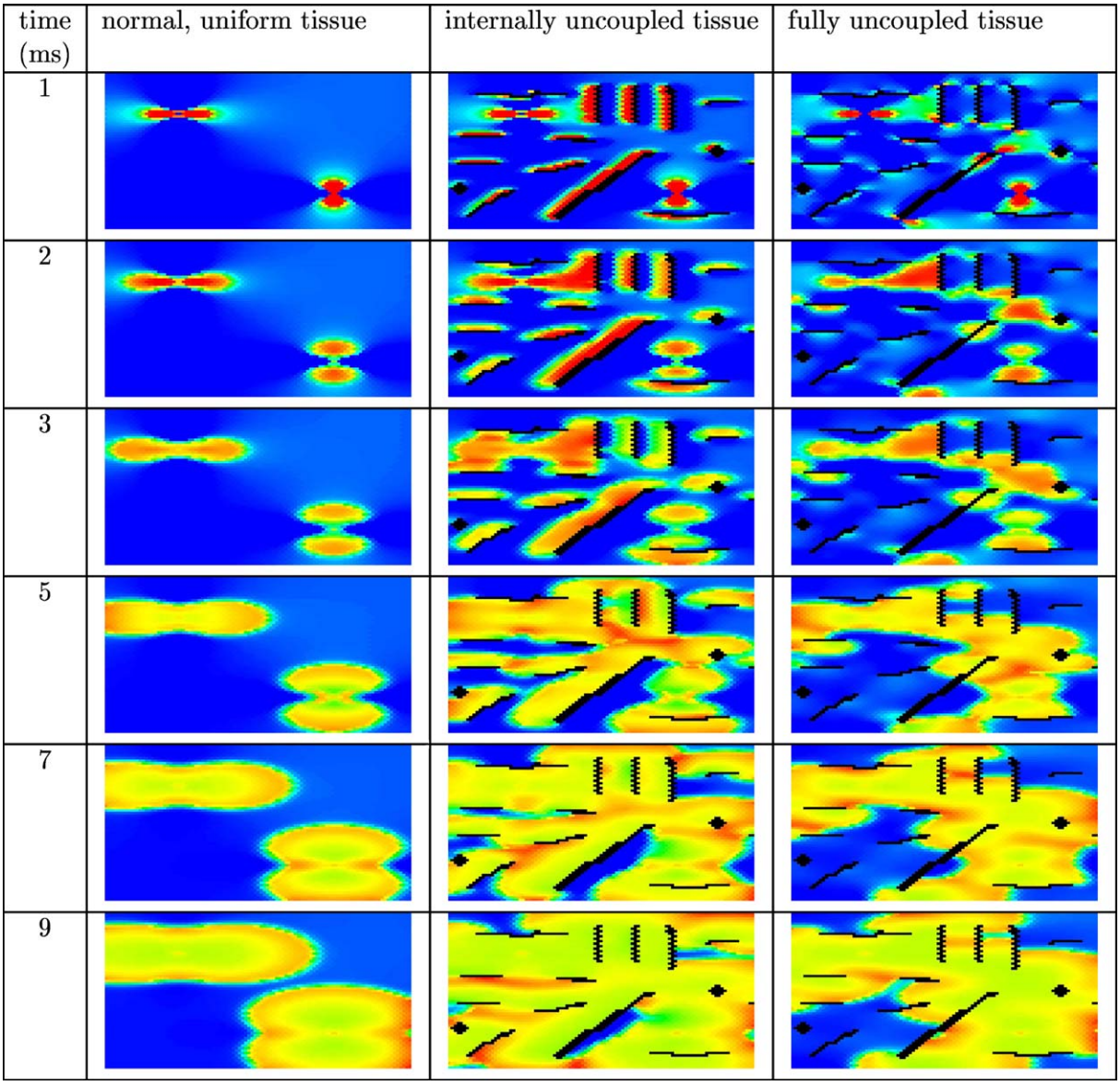

Figure 2 Anodal and cathodal point stimulation in uniform (left column), internally uncoupled (centre column) and fully uncoupled (right column) resting cardiac tissue. The anode is located in the upper left quarter and the cathode in the lower right quarter of the tissue. Artificial obstacles are created by (internally) uncoupling the black bricks from the surrounding tissue. An electric field was applied during the first millisecond of the simulation. Shown are the membrane potentials for different simulation times after field stimulation. Depolarized tissue is coloured light and hyperpolarized or resting tissue dark.

entire tissue is more rapidly depolarized. In remodelled tissue (see Fig. 5) more virtual electrodes are created compared with normal, non-uniform tissue. However, since the velocity of the wavefront is lower compared with normal tissue, it takes more time to depolarize the entire tissue.

In Fig. 6 the results are shown when an electric field is applied in uniform and non-uniform normal tissue in which a spiral wave was induced. The spiral wave is not terminated in uniform atrial tissue (left column). As before, more virtual electrodes originate in the bulk of non-uniform tissue (centre and right column). Virtual electrodes can be observed in both the excitable gap and depolarized tissue. In the centre column the number of virtual electrodes in the excitable gap is too small to terminate the spiral wave. However, in the right column, more virtual electrodes are present in the excitable gap and the spiral wave is terminated. The entire tissue recovers and no activity is left to initiate new depolarization waves.

Downloaded from by guest on July 25, 2016

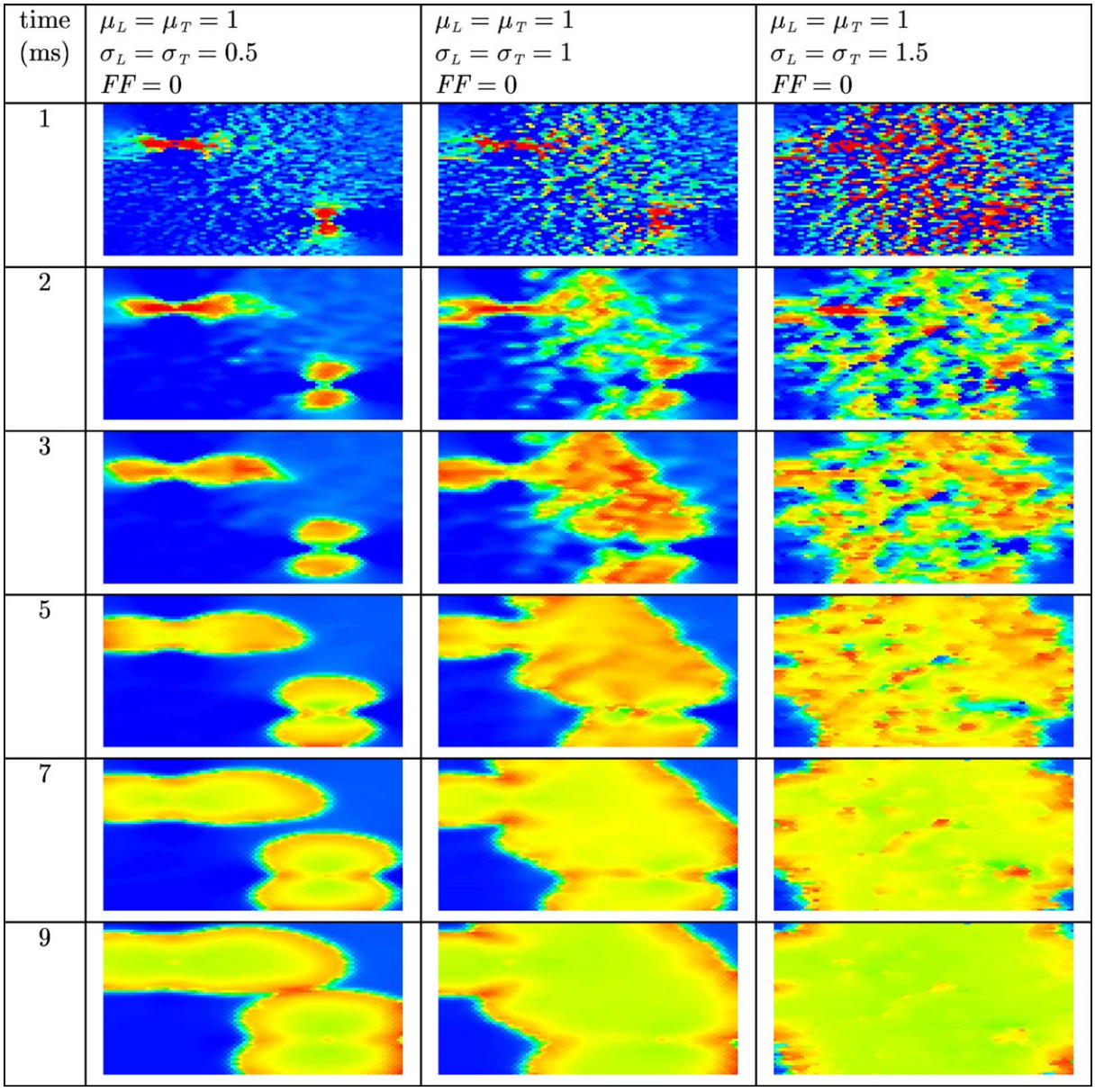

Figure 3 Anodal and cathodal point stimulation in resting cardiac tissue with non-uniform internal conductivity. The anode is located in the upper left quarter and the cathode in the lower right quarter of the tissue. An electric field was applied during the first millisecond of the simulation. Shown are the membrane potentials for different simulation times after field stimulation. Depolarized tissue is coloured light and hyperpolarized or resting tissue dark.

Also in Fig. 7 virtual electrode polarization is clearly visible in remodelled tissue and the spiral wave is terminated. Compared with normal, non-uniform tissue more virtual electrodes are present. However, since the propagation of the action potential is slower in remodelled tissue, the time it takes to depolarize the entire tissue is longer compared with the time it takes to depolarize normal, non-uniform tissue. The membrane potentials of 10 different bricks are shown in Fig. 8. These bricks are located in the same row in the centre of the tissue, thus the distance to the anode and cathode is the same for each brick. The dashed lines represent the time when the cell recovers. All cells recover between approximately 180 and 320 ms after the electric field is applied. Note the different shapes of the APs, as these are either prolonged or shortened due to the virtual electrodes. This mechanism leads to total recovery of the tissue within a time window of approximately 140 ms, regardless of whether the nodes are depolarized or resting at the time the electric field is applied.

Downloaded from by guest on July 25, 2016

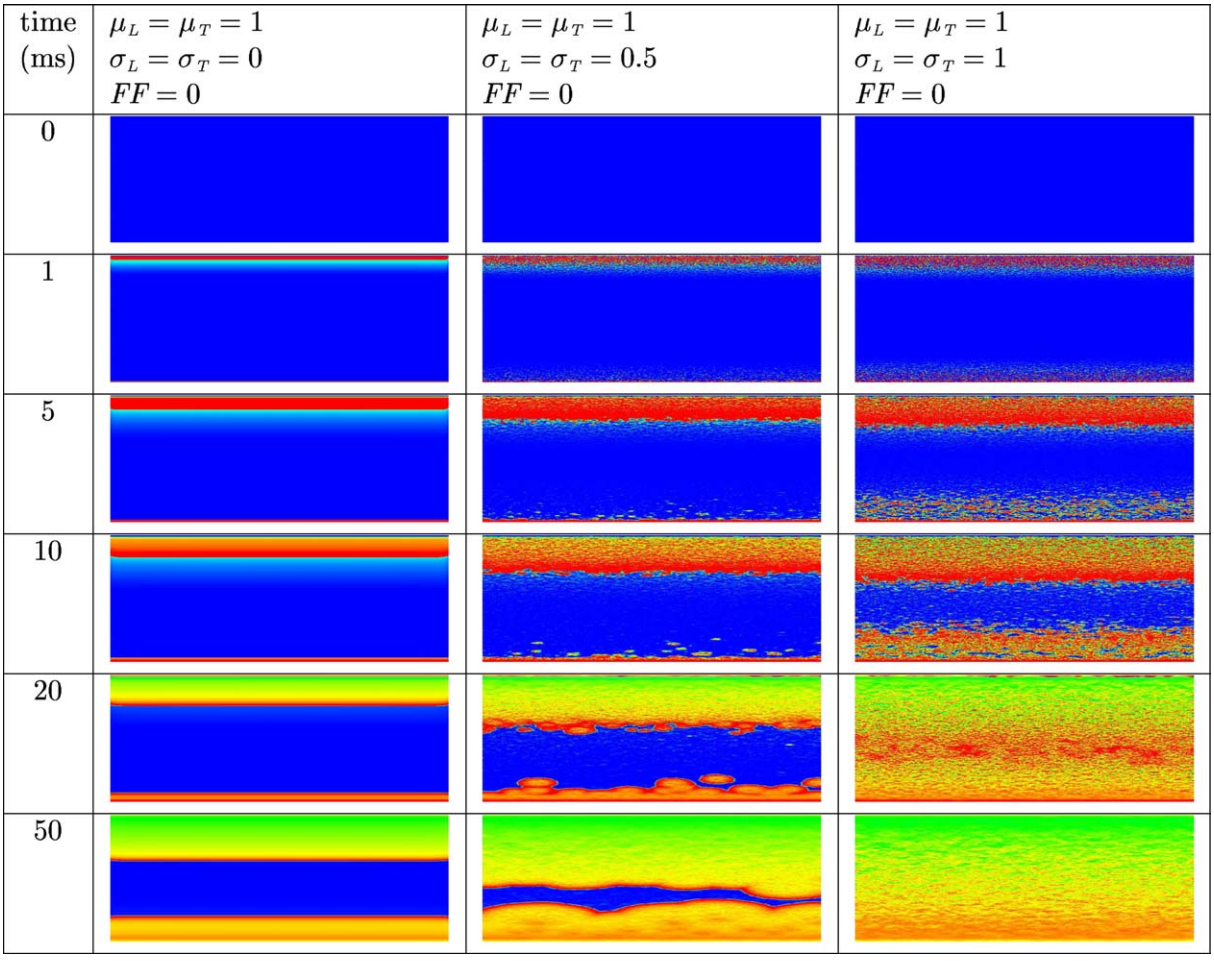

Figure 4 Virtual electrode polarization in uniform (left column) and non-uniform (centre column and right column) resting cardiac tissue. The anode was a line electrode at the top and the cathode a line electrode at the bottom of the tissue. A uniform electric field was applied during 10 ms. Shown are the membrane potentials for different simulation times during and after field stimulation. Depolarized tissue is coloured light and hyperpolarized or resting tissue dark.

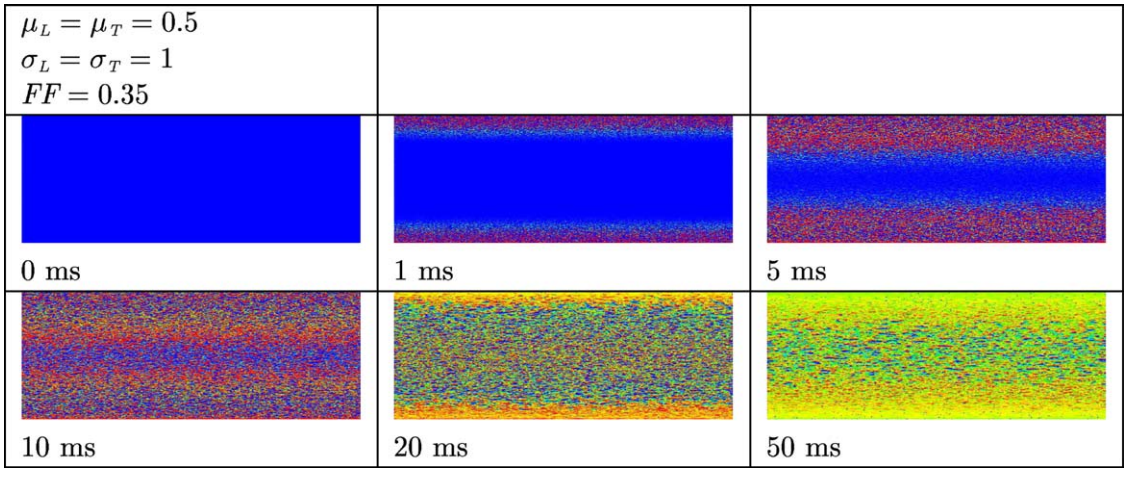

Figure 5 Virtual electrode polarization in resting remodelled tissue. The anode was a line electrode at the top and the cathode a line electrode at the bottom of the tissue. A uniform electric field was applied during 10 ms. Shown are the membrane potentials for different simulation times during and after field stimulation. Depolarized tissue is coloured light and hyperpolarized or resting tissue dark.

Downloaded from by guest on July 25, 2016

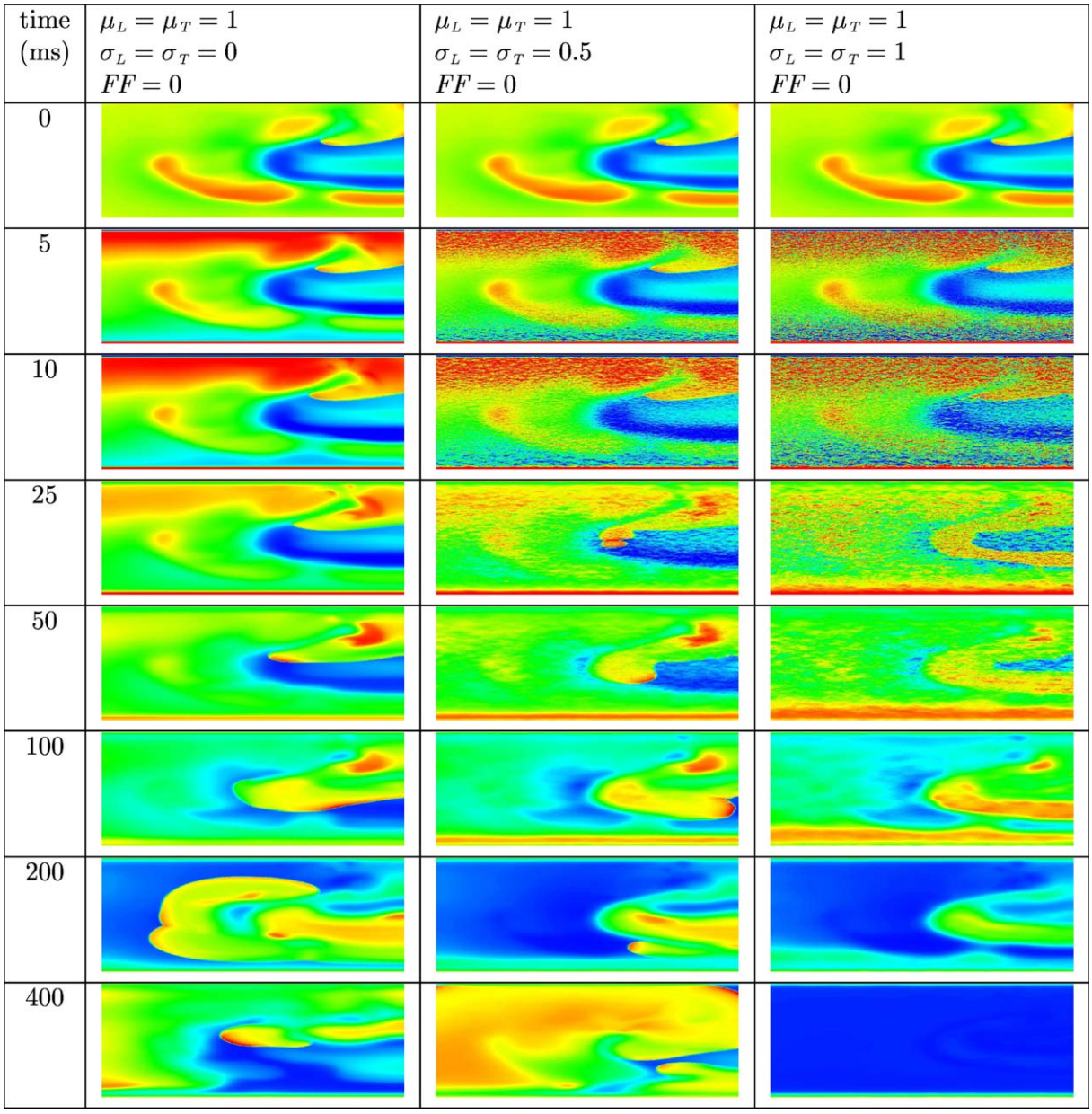

Figure 6 Unsuccessful and successful termination of a spiral wave in uniform (left column) and non-uniform (centre and right column) tissue by means of defibrillation. The anode was a line electrode at the top and the cathode a line electrode at the bottom of the tissue. A uniform electric field was applied during 10 ms. Shown are the membrane potentials for different simulation times during and after field stimulation. Depolarized tissue is coloured light and repolarized or hyperpolarized tissue dark.

Discussion

Cellular Bidomain Model

To simulate cardiac electrical behaviour cardiac tissue is traditionally modelled either by a continuous model such as the bidomain equations [36] or a discontinuous model such as the parallel cable model [37]. The latter allows for the modelling of tissue at subcellular level. The parallel cables can be connected in a brick wall fashion as described in Ref. [37]. In recent studies to field stimulation, spatial heterogeneity is introduced in bidomain models in which the cells are subdivided and gap junctions are modelled explicitly [17–19]. In the Cellular Bidomain Model the bricks are not subdivided. Both the intracellular and extracellular domains can be viewed as a hexagonal grid of resistors. Non-uniformity is modelled by varying the intracellular resistances and decoupling is

Downloaded from by guest on July 25, 2016

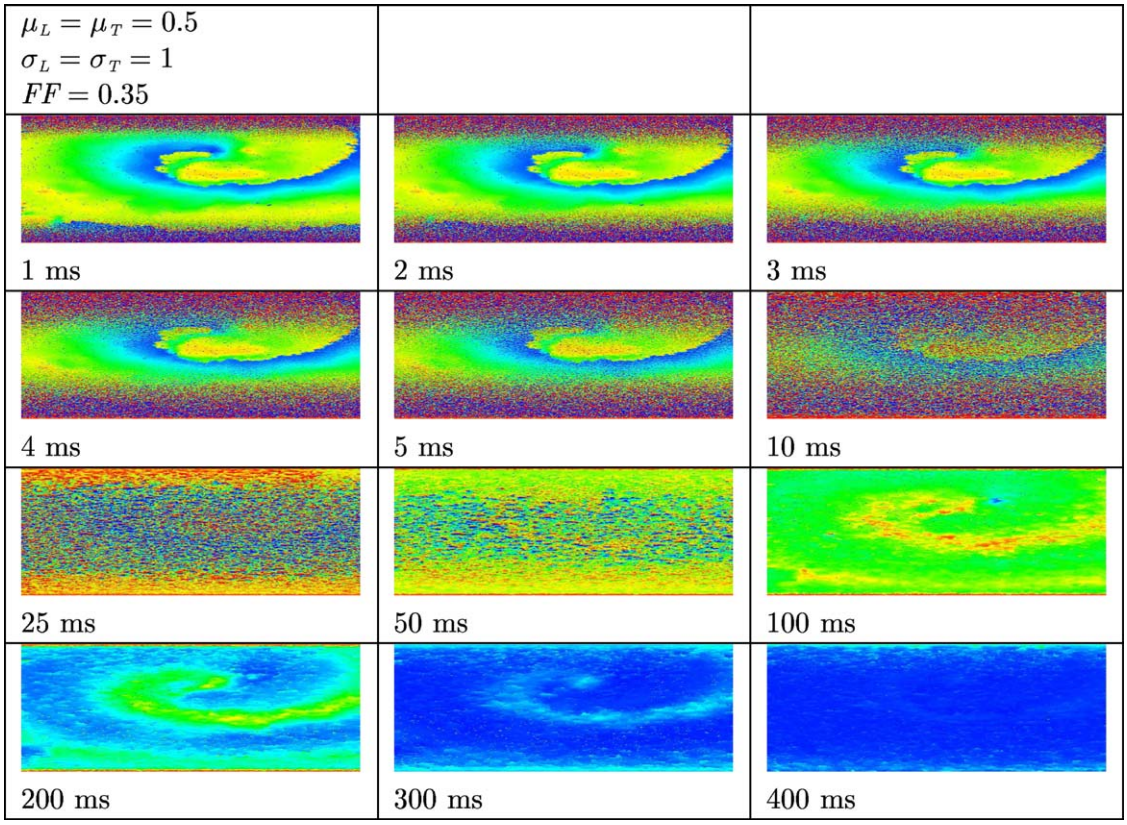

Figure 7 Termination of a spiral wave in remodelled tissue by means of defibrillation. The anode was a line electrode at the top and the cathode a line electrode at the bottom of the tissue. A uniform electric field was applied during 10 ms. Shown are the membrane potentials for different simulation times during and after field stimulation. Depolarized tissue is coloured light and repolarized or hyperpolarized tissue dark.

modelled by disconnecting some of the intracellular resistors randomly. Using a brick wall structure composed of bricks of length 200 μm and width 80 μm and experimentally measured conductivities that are all scaled with the same factor leads to conduction velocities that are in physiological range.

In the present study, the effects of a surrounding conductive bath and fibre curvature are not investigated. We expect that the results would not change qualitatively if the sheets of cardiac tissue were surrounded by a conductive bath (see e.g. the simulation study by Plank et al. [21]). The influence of fibre curvature when an electric field is applied has been thoroughly investigated in 2D and 3D by the group of Trayanova [12,13, 22,38,39].

Virtual electrode polarization

By establishing an external electric field, virtual electrodes are formed which either depolarize or hyperpolarize regions in the cardiac tissue [5]. From our simulation results we conclude that decoupling and non-uniform conductivity affects the virtual electrode polarization (VEP). In decoupled and non-uniform tissue virtual electrodes appear in the bulk of the tissue and depolarize all excitable parts of the tissues within short time. A spiral wave can be terminated when the excitable gap is depolarized and no excitable tissue is left.

Pathological tissue

We simulated pathological tissue by modelling diffuse fibrosis and remodelling of the gap junctions. An important difference between normal, non-uniform and remodelled tissue is the reduction in conduction velocity. Since the success of defibrillation depends on the fast depolarization of the entire tissue, a slower conduction velocity might lead to defibrillation failure. Virtual electrodes can occur near obstacles such as scars caused by infarction or surgical incisions [15]. If the virtual electrodes are not well-spread throughout the tissue, these obstacles might in fact form a substrate for arrhythmogenesis [15]. This mechanism can also be observed in Fig. 2. The presence of

Downloaded from by guest on July 25, 2016

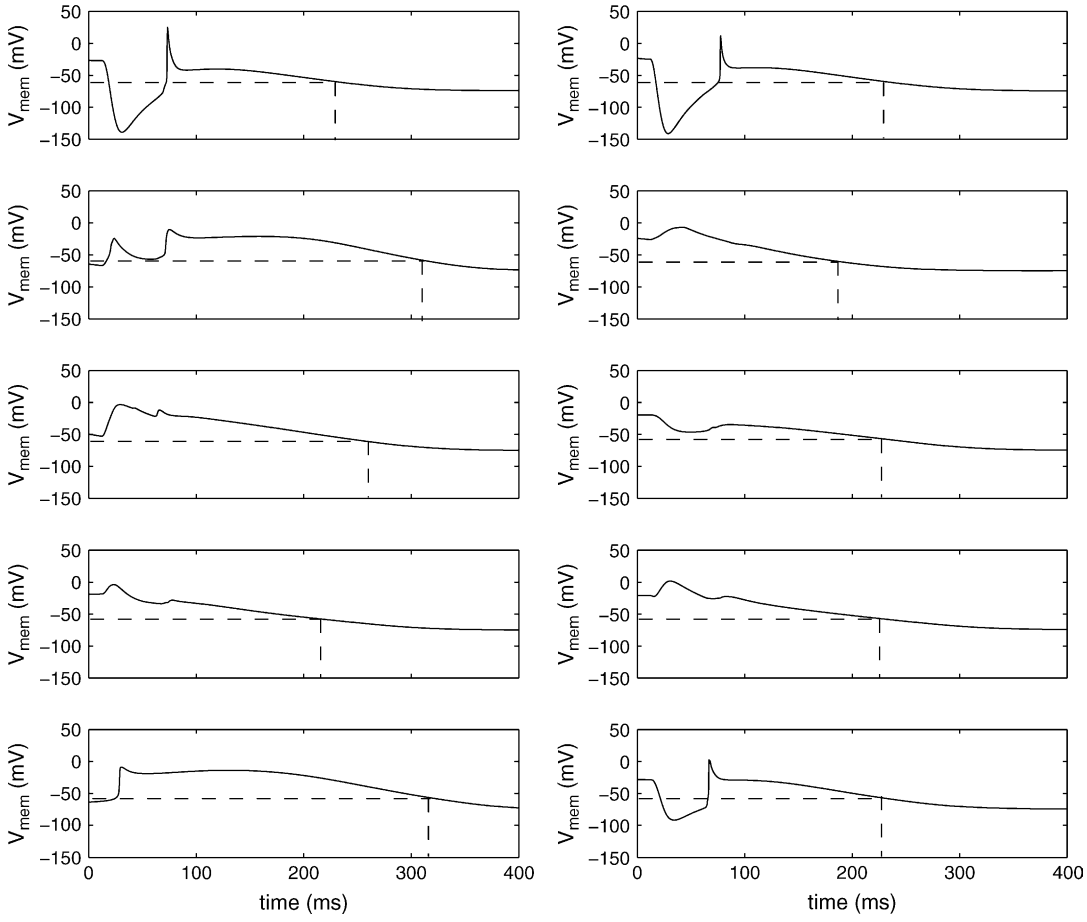

Figure 8 Prolonging and shortening of action potentials in remodelled tissue. Shown are the membrane potentials of 10 different bricks lying on one line in the centre of the tissue. The membrane potentials are shown starting 10 ms before application of the electric field. The dashed lines represent the recovery times.

virtual electrodes is determined by the location of non-conductive obstacles. Obstacles that are non-conductive in both domains lead to a different pattern of virtual electrode polarization compared with obstacles that are non-conductive in the internal domain only. In case of low conduction velocities, localized regions of depolarization might be a substrate for new fibrillating waves.

Conclusion

We have simulated sheets of normal and pathological atrial tissue on which an external electric field was established. To introduce spatial heterogeneity and to simulate the effects of gap junction remodelling and diffuse fibrosis, local conductivities were varied throughout the tissue. Using this model we investigated the role of non-uniform conductivities in relation to virtual electrode polarization on resting cardiac tissue as well as tissue in which spiral waves were induced. From the simulation results we conclude that successful termination of spiral waves depends on the amount and spread of virtual electrodes. Compared with normal, non-uniform tissue, more virtual electrodes are present in the bulk of remodelled tissue. However, since the conduction velocity in remodelled tissue is lower, it takes more time to depolarize the entire tissue. We conclude that fast depolarization of the tissue after field stimulation may be explained by intracellular decoupling and spatial heterogeneity present in normal and pathological cardiac tissue. We demonstrated that termination of spiral waves by means of field stimulation can be achieved when the tissue is modelled as a non-uniform, anisotropic bidomain with active membrane behaviour.

References

[1] Efimov IR, Cheng Y, Van Wagoner DR, Mazgalev T, Tchou PJ. Virtual electrode-induced phase singularity: a basic mechanism of defibrillation failure. Circ Res 1998; 82:918—25.

Downloaded from by guest on July 25, 2016

[2] Efimov IR, Cheng YN, Yamanouchi Y, Tchou PJ. Direct evidence of the role of virtual electrode-induced phase singularity in success and failure of defibrillation. J Cardiovasc Electrophysiol 2000;11:861—8.
[3] Efimov IR, Aguel F, Cheng Y, Wollenzier B, Trayanova N. Virtual electrode polarization in the far field: implications for external defibrillation. Am J Physiol Heart Circ Physiol 2000;279:H1055—70.
[4] Roth BJ, Wikswo Jr JP. Electrical stimulation of cardiac tissue: a bidomain model with active membrane properties. IEEE Trans Biomed Eng 1994;41:232—40.
[5] Wikswo Jr JP, Lin SF, Abbas RA. Virtual electrodes in cardiac tissue: a common mechanism for anodal and cathodal stimulation. Biophys J 1995;69:2195—210.
[6] Newton JC, Knisley SB, Zhou X, Pollard AE, Ideker RE. Review of mechanisms by which electrical stimulation alters the transmenbrane potential. J Cardiovasc Electrophysiol 1999;10:234—43.
[7] Trayanova N. Discrete versus syncytial tissue behavior in a model of cardiac stimulation — II: results of simulation. IEEE Trans Biomed Eng 1996;43:1141—50.
[8] Keener JP, Panfilov AV. A biophysical model for defibrillation of cardiac tissue. Biophys J 1996;71:1335—45.
[9] Krassowska W, Neu JC. Response of a single cell to an external electric field. Biophys J 1994;66:1768—76.
[10] Zhou X, Ideker RE, Blitchington TF, Smith WM, Knisley SB. Optical transmembrane potential measurements during defibrillation-strength shocks in perfused rabbit hearts. Circ Res 1995;77:593—602.
[11] Gillis AM, Fast VG, Rohr S, Kléber AG. Spatial changes in transmembrane potential during extracellular electrical shocks in cultured monolayers of neonatal rat ventricular myocytes. Circ Res 1996;79:676—90.
[12] Trayanova N, Skouibine K, Aguel F. The role of cardiac tissue structure in defibrillation. Chaos 1998;8:221—33.
[13] Trayanova N, Skouibine K. Modeling defibrillation: effects of fiber curvature. J Electrocardiol 1998;31:23—9.
[14] Fast VG, Rohr S, Gillis AM, Kléber AG. Activation of cardiac tissue by extracellular electrical shocks. Circ Res 1998;82:375—85.
[15] White JB, Walcott GP, Pollard AE, Ideker RE. Myocardial discontinuities: a substrate for producing virtual electrodes that directly excite the myocardium by shocks. Circulation 1998;97:1738—45.
[16] Hooks DA, Tomlinson KA, Marsden SG, LeGrice IJ, Smaill BH, Pullan AJ, et al. Cardiac microstructure implications for electrical propagation and defibrillation in the heart. Circ Res 2002;91:331—8.
[17] Fishler MG. Syncytial heterogeneity as a mechanism underlying cardiac far-field stimulation during defibrillation-level shock. J Cardiovasc Electrophysiol 1998;9:384—94.
[18] Fishler MG. Spatiotemporal effects of syncytial heterogeneities on cardiac far-field excitations during monophasic and biphasic shocks. J Cardiovasc Electrophysiol 1998;9:1310—24.
[19] Krassowska W. Field stimulation of cardiac fibers with random spatial structure. IEEE Trans Biomed Eng 2003;50:33—40.
[20] Keener JP, Cytrynbaum E. The effect of spatial scale of resistive inhomogeneity on defibrillation of cardiac tissue. J Theor Biol 2003;223:233—48.
[21] Plank G, Leon LJ, Kimber S, Vigmond EJ. Defibrillation depends on conductivity fluctuations and the degree of disorganization in reentry patterns. J Cardiovasc Electrophysiol 2005;16:205—16.
[22] Hillebrenner MG, Eason JC, Trayanova NA. Mechanistic inquiry into decrease in probability of defibrillation success with increase in complexity of preshock reentrant activity. Am J Physiol Heart Circ Physiol 2004;286:H909—17.
[23] Courtemanche M, Ramirez RJ, Nattel S. Ionic mechanisms underlying human atrial action potential properties: insights from a mathematical model. Am J Physiol 1998;275:H301—21.
[24] Aguel F, Katherine BS, Debruin A, Krassowska W, Trayanova NA. Effects of electroporation on the transmembrane potential distribution in a two-dimensional bidomain model of cardiac tissue. J Cardiovasc Electrophysiol 1999;10:701—14.
[25] Luo C, Rudy Y. A dynamic model of the cardiac ventricular action potential. Circ Res 1994;74:1071—96.
[26] Beeler GW, Reuter H. Reconstruction of the action potential of ventricular myocardial fibers. J Physiol 1977;268:177—210.
[27] Spach MS, Boineau JP. Microfibrosis produces electrical load variations due to loss of side-to-side cell connections: a major mechanism of structural heart disease arrhythmias. Pacing Clin Electrophysiol 1997;20:397—413.
[28] Clerc L. Directional differences of impulse spread in trabecular muscle from mammalian heart. J Physiol 1976;255:335—46.
[29] Krassowska W. Effects of electroporation on transmembrane potential induced by defibrillation shocks. Pacing Clin Electrophysiol 1995;18:1644—60.
[30] Al-Khadra A, Nikolski V, Efimov IR. The role of electroporation in defibrillation. Circ Res 2000;87:797—804.
[31] Skouibine K, Trayanova N, Moore P. A numerically efficient model for simulation of defibrillation in an active bidomain sheet of myocardium. Math Biosci 2000;166:85—100.
[32] Jongsma HJ, Wilders R. Gap junctions in cardiovascular disease. Circ Res 2000;86:1193—7.
[33] Spach MS, Heidlage JF. The stochastic nature of cardiac propagation at a microscopic level: electrical description of myocardial architecture and its application to conduction. Circ Res 1995;76:366—80.
[34] Fast VG, Kléber AG. Block of impulse propagation at an abrupt tissue expansion: evaluation of the critical strand diameter in 2- and 3-dimensional computer models. Cardiovasc Res 1995;30:449—59.
[35] Kawara T, Derksen R, De Groot J, Coronel R, Tasseron SRT, Linnenbank AC, et al. Activation delay after premature stimulation in chronically diseased human myocardium relates to the architecture of interstitial fibrosis. Circulation 2001;104:3069—75.
[36] Henriquez CS. Simulating the electrical behavior of cardiac tissue using the bidomain model. Crit Rev Biomed Eng 1993;21:1—77.
[37] Leon LJ, Roberge FA. Structural complexity effects on transverse propagation in a two-dimensional model of myocardium. IEEE Trans Biomed Eng 1991;38:997—1009.
[38] Eason J, Trayanova N. Phase singularities and termination of spiral wave reentry. J Cardiovasc Electrophysiol 2002;13:672—9.
[39] Rodríguez B, Trayanova N. Upper limit of vulnerability in a defibrillation model of the rabbit ventricles. J Electrocardiol 2003;36:51—6.

Downloaded from by guest on July 25, 2016